COMPARISON OF DIGITAL TERRAIN MODELS FROM TWO PHOTOCLINOMETRY METHODS

R. L. Kirk [1] *, D. P. Mayer [1], C. M. Dundas [1], B. H. Wheeler [1], R. A. Beyer [2, 3], O. Alexandrov [3]

[1] U.S. Geological Survey, Astrogeology Science Center, Flagstaff, Arizona, USA - (rkirk, dpmayer, cdundas, bhwheeler)@usgs.gov
[2] SETI Institute, Mountain View, California, USA - rbeyer@seti.org
[3] NASA Ames Research Center, Moffett Field, California, USA - oleg.alexandrov@nasa.gov

Commission III, ICWG III/2

KEY WORDS: Moon, DTMs, quality control, photoclinometry, shape-from-shading

ABSTRACT:

We evaluate the horizontal resolution and vertical precision for digital topographic models (DTMs) of the Moon derived from image radiance information, a process known as photoclinometry (PC) or shape-from-shading (SfS). We use the implementations in two available planetary image processing software systems, single image PC in the U.S. Geological Survey Integrated Software for Imagers and Spectrometers (ISIS) system, and multi-image SfS in the Ames Stereo Pipeline (ASP), and test results obtained with and without use of a starting solution from stereo, with single and multiple images, and for varying illumination conditions. To obtain the higher quality reference DTMs against which the products can be evaluated, we derived DTMs by stereoanalysis of Lunar Reconnaissance Orbiter Narrow-Angle Camera (LROC NAC) images at their native pixel spacing of ~0.5 m, then produced a 16-m/post stereo DTM from images downsampled to 4 m/pixel and refined it with images at 16 m/pixel. When used with a single image, both algorithms improved resolution (by a factor of 1.4 for PC and 2.4 for SfS compared to stereo). An albedo map produced in ISIS by ratioing the image to a simulation based on the stereo DTM was well correlated with one output by SfS. The albedo correction was crucial for PC with ~60° incidence but not at ~80°. DTMs produced by PC and SfS without a starting stereo DTM had larger errors but good detail, and could be useful for many applications. In SfS, it was necessary to increase smoothing to get a usable DTM when the weighting on an *a priori* DTM was reduced. Multi-image SfS including modeling of spatially varying albedo reduced vertical errors by factors of 1.5 or more compared to single-image SfS.

1. INTRODUCTION

Topography is a foundational dataset for planetary science (Laura and Beyer, 2021) with a wide range of applications from mission planning to qualitative and quantitative data analysis. A commonly used method for deriving high density digital topographic models (DTMs) is stereogrammetry, which is based on geometric comparison of two (or more) images acquired from different viewing angles. An alternative approach is photoclinometry (PC), also called shape-from-shading (SfS; the two terms are synonymous but we will use them below to distinguish the two software implementations under study by the names their developers used). Such methods, which are based on image radiance rather than geometry, offer the prospect of higher spatial resolution matching the pixel scale of individual images, but they require information about the surface photometric function. The applicability of radiance-based methods to single images is a considerable advantage, but if variations in surface reflectivity (albedo) are large and are not corrected for—by using multiple images with different illumination or by some other means—the resulting DTMs can be distorted. Our goal is to measure the quality of DTMs produced or enhanced by PC/SfS with different software implementations and input data.

The work reported here builds on our past efforts to assess the quality of "target" DTMs made by various approaches by comparing them to precisely registered "reference" DTMs. Specifically, by differencing the target DTM with versions of the reference smoothed to varying degrees, as described in Section 3.1 below, it is possible to estimate the horizontal resolution and the vertical precision of the target. Kirk et al. (2016) used this approach to evaluate the quality of stereo DTMs produced from simulated images of Europa by using the commercial photogrammetric system SOCET SET©† (Miller and Walker, 1993, 1995). The known DTM used as the input for creating the simulated images served as the reference in that work, which focused on the variation of stereo DTM quality with illumination and differences in illumination between the paired images. More recently, Kirk et al. (2021) used DTMs of Mars generated from High Resolution Imaging Science Experiment (HiRISE; McEwen et al., 2007) images at a ground sample distance (GSD) of ~25 cm/pixel as the reference for evaluating DTMs made from images from the High Resolution Stereo Camera (HRSC, with stereo channel GSD 25 m or greater; Neukum and Jaumann, 2004) and Context Camera (CTX, with GSD ~6 m; Malin et al., 2007). Kirk et al. (2021) evaluated DTMs produced with SOCET SET and with several stereo matching algorithms available in the Ames Stereo Pipeline (ASP). They focused on the scaling of resolution and precision with image GSD and the effect of processing parameters on these quality metrics. They showed that refining a stereo DTM by PC could improve its horizontal resolution by a factor of 2–3, with little effect on vertical error. Finally, Bland et al. (2021) assessed the quality of Europa DTMs made from real Galileo SSI stereopairs (Belton et al., 1992). Lacking a suitable reference dataset of higher quality, they estimated horizontal resolution visually, and used the RMS difference between DTMs made from the same stereopair in SOCET SET and ASP as a proxy for vertical precision. Their results were nevertheless broadly consistent with those of the earlier two studies, when appropriately normalized by the image GSD.

* Corresponding author
† Any use of trade, firm, or product names is for descriptive purposes only and does not imply endorsement by the U.S. Government.

In this paper, we compare the performance of two planetary remote sensing and mapping software packages that create radiance-based DTMs: the multi-image *sfs* tool (Alexandrov and Beyer, 2018) in ASP version 3.0.0 (Beyer et al., 2021) and the single-image *pc2d/pcsi* code (Kirk et al., 2003a) implemented in ISIS2 (the Integrated Software for Imagers and Spectrometers, version 2.x; Gaddis et al., 1997). ISIS2 has since been superseded by a series of newer versions beginning with a complete redesign in ISIS 3.0 (Anderson et al., 2004; Sides et al., 2017). Although much of the earlier functionality of ISIS is available in the redesigned system, the photoclinometry capabilities are not.

Our primary goal is to evaluate how refining stereo DTMs by using the two methods affects (and hopefully improves) the resolution and precision achievable by stereo. We use images of Earth's Moon for this investigation because of the availability of extensive high-resolution coverage that includes both stereo and diverse illumination conditions. The scientific and programmatic interest in topographic mapping of the Moon is also a motivation. Among the questions we seek to answer are the following:

- How do the results of the two methods compare when they are applied to the same data?
- How does the achievable DTM quality vary with illumination (specifically, with incidence angle for a single image)?
- What are the appropriate processing parameters for the two algorithms, including the optimal stopping criterion for iteration, the weighting favoring a smoother DTM, and (for *sfs*) the weighting favoring similarity to *a priori* low-resolution topographic information?
- What is the quality of DTMs produced *ab initio* by PC or SfS? Are the effects of illumination or of processing parameters different than when a stereo DTM is used as a starting point for iteration? Can the methods provide useful information in the many areas lacking stereo coverage?
- How is the quality of results from *sfs* affected when multiple images are available? How does this depend on illumination (i.e., on relative sun azimuths as well as incidence angles)? Do the processing parameters need to be adjusted?

2. DATA

The images of the Moon used in this study were obtained by the Lunar Reconnaissance Orbiter Camera Narrow Angle Camera (LROC NAC, henceforth NAC for brevity; Robinson et al., 2010) on the National Aeronautics and Space Administration (NASA) Lunar Reconnaissance Orbiter (LRO). This system consists of two identical pushbroom scanning cameras whose fields of view are adjacent (with slight overlap) in the across-track direction. At the nominal orbit altitude for much of the LRO mission, the images have a GSD of ~0.5 m/pixel and a combined swath width of ~5 km. Most images are acquired while the spacecraft is nadir-pointed; stereo coverage can be obtained by rotating off nadir to target the same location on separate orbits. Among the numerous lunar features observed with the NAC, the 50 regions of interest defined by the former NASA Constellation Program were targeted repeatedly, resulting in extensive overlapping coverage of single images and stereopairs with varying illumination (Gruener and Joosten, 2009). Images with large solar incidence angles (although not so large that extensive shadows result) are desirable for PC/SfS methods because the oblique illumination emphasizes topographic shading and minimizes the visibility of albedo variations. We therefore selected two study sites at high southern latitudes, where images with appropriate incidence angles and a wide range of sun azimuths are available.

At the Schrödinger site (SCH, centered at 138.77°E, 75.40°S) we identified a cluster of 174 images with incidence angles from 72° to 85° and sun azimuths from -70° to 70° relative to north. This cluster includes 5 targeted stereopairs and a total of 16 images with emission angles ≥10° that could provide additional stereo coverage. Images M123681855 and M123668289, a targeted stereopair with emission angles of 14.21° to the west and 5.33° to the east (for a parallax to height ratio p/h of 0.347) were used to create the reference and initial DTMs, and the less-oblique second image was used for PC/SfS. The phase angle, incidence angle and sun azimuth clockwise from north for this image are 77.94°, 76.92°, and -10.30°. An overlapping pair, M141337621 and M141364760, with p/h = 0.447 was used to create a second stereo DTM as an independent check on the first pair.

The South Pole-Aitkin Basin site (SPA, centered at 200.06°E, 60.00°S) includes a cluster of 80 overlapping images with incidence angles from 58° to 85° and sun azimuths in the range -84° to 81°. This set includes 5 targeted stereopairs and 11 images with emission angles greater than 10°. The targeted stereopair used to make reference and initial DTMs consists of images M1117572011 and M1117557807, with emission angles 17.89° to the west and 12.76° to the east (p/h = 0.549). The less oblique second image, used for PC/SfS, has phase, incidence, and solar azimuth angles of 62.75°, 61.46°, and 1.25°. We refer to it as image "N" below. Two additional images overlapping this pair were selected for multi-image SfS: M1158818485 ("W," incidence 75.18°, sun azimuth -66.24°) and M114994918 ("E," incidence 79.34°, azimuth 72.80°).

3. METHODS

3.1 Quality Assessment

Our primary approach to quality assessment involves comparing a target DTM to a precisely coregistered reference DTM derived from images with much smaller GSD. Because DTM resolution and precision are both generally proportional to image GSD (Kirk et al., 2021), errors in the reference contribute little to the difference between the two products. Instead, the dispersion of difference values can be attributed to some combination of vertical errors in the target and the presence of small (real) features in the reference that the target DTM fails to resolve. Because we are interested in relative errors (precision) rather than absolute elevation offsets, we use the standard deviation of the difference as a dispersion measure. This is equivalent to the root mean squared (RMS) difference after adjusting the two datasets to have the same mean. We also exclude some outliers that are associated with spike-like artifacts in the shadowed areas of the reference DTM.

To distinguish the effect of resolution from that of precision, we difference the target DTM with versions of the reference that have been smoothed with lowpass boxcar filters of increasing size. The filter size at which the RMS difference is a minimum, indicating a balance between suppressing features that are absent from the target and those that are present, provides an estimate of the horizontal resolution of the target DTM. The width of the optimal boxcar filter is only one of several ways of quantifying resolution, but it is well correlated with other measures (Kirk et al., 2021) so for brevity we call it "resolution" below. The RMS difference at this filter scale is an estimate of the vertical precision of the target.

Note that we compare the quality *statistics* of the refined DTMs to those of the initial (coarse) stereo solution below, but in every case the quality of a DTM is assessed by comparing it to the reference model.

3.2 Data Preparation

The one or two stereopairs needed to create reference DTMs and the limited number of additional images to be used for multi-image SfS at each site must be precisely coregistered by

photogrammetric bundle adjustment (BA). Because matching corresponding features (an essential input for BA) in images with widely varying illumination is extremely difficult, we included the complete set of overlapping images in the matching and adjustment process; the extra images with intermediate illumination directions provide a "bridge" between those to be used in the later analysis (Beyer et al., 2021, Section 11.4). A relative BA (based on image to image ties but without image to ground control points) was performed for each site by using the ISIS adjustment program *jigsaw* (Edmundson et al., 2012).

A limitation of our approach is that no lunar topographic dataset is suitable as a reference for evaluating DTMs made from the 0.5 m/pixel NAC images; a few Apollo surface observations with higher resolution exist, but only over limited areas in the equatorial zone where the illumination conditions are less favorable for PC/SfS. We therefore adopted the approach of Alexandrov and Beyer (2018) for deriving reference and target DTMs from the same images processed at full and reduced GSD. At both scales, stereo processing was performed with the ASP module *parallel_stereo* with block matching and subpixel refinement, which yields DTMs with a resolution of about 16 image pixels (Kirk et al., 2021, confirmed for reduced NAC images in Section 4.1). DTMs were made from 0.5 m/pixel images with a GSD of 2 m and resampled to 16 m to provide a reference with full one-post resolution. Initial target DTMs to be refined by PC/SfS were produced at the same 16-m GSD by stereoanalysis of images at 4 m/pixel, yielding resolutions on the order of 4 posts as shown below. The 4-m images were further downsampled to match the 16-m GSD of the DTM before being used in the PC/SfS algorithms. Using images with pixels smaller than the DTM yields noisy results as a consequence of aliasing, and should be avoided.

The process just described corresponds to a realistic workflow that might be used if 4 m/pixel images from a real camera were available. A stereo DTM would normally be produced with a GSD in the range 3–5 pixels, smaller than the actual resolution. A conservative first step in making use of PC/SfS would then be to refine the DTM at the same GSD, to try to obtain a resolution closer to the sample spacing. In the present study, we focus on this problem and show that resolution can indeed be improved even though we have reduced the images from 4 to 16 m/pixel.

Radiance-based methods offer the prospect of refining the DTM resolution all the way to that of the available images, but we leave such tests for future work. In a real-world scenario with 4 m/pixel images, this would mean enlarging the stereo DTM to 4 m/post (or making it at that GSD initially) and refining it with the 4-m image(s). Conversely, to do a test that could be evaluated with a 16-m reference DTM one would need to start with a stereo DTM made from 16 m/pixel images. We have not attempted this, but confidently expect it would yield substantially greater improvements in resolution than reported here.

A photometric model is required in order to carry out PC or SfS. The default model in *sfs* is a lunar-Lambert empirical function (McEwen, 1991) with limb-darkening parameter L expressed as a polynomial function of phase angle, based on fits to Clementine images of the Moon by McEwen et al. (1995). We therefore used the same function and phase-appropriate L value for PC as well. Note that this polynomial is specific to the Moon and is not an appropriate default for other bodies. Also, the paper by McEwen et al. (1995) from which the fit is taken erroneously includes an older form of the lunar-Lambert model. McEwen (written communication, 2021) has confirmed that this is a typographical error. The definition of McEwen (1991), in which the lunar term is multiplied by $2L$ rather than L, should be used with the fit. Both ASP and ISIS use this definition.

3.3 Photoclinometry

The research software (Kirk, 1987, Part III) on which the ISIS implementation of PC (Kirk et al., 2003a) was based was intended for use with single images in an era when planetary stereo coverage was limited. The surface model is defined in camera-centered coordinates, with "elevation" measured toward the camera, but as a special case, when an orthoimage is used, the model is a standard DTM with elevation measured vertically. The correct (not necessarily vertical) emission direction is used in the photometric model in this case. With only a single input, the algorithm solves for elevations under the assumption that the albedo is uniform (or has been corrected for by pre-processing the image). There is thus a tradeoff between a desire for larger incidence angles to maximize the contrast of topographic shading to minimize the effect of albedo variations and the desire to avoid shadowing.

Image data must be available for every pixel, so for this project we selected a 4x20-km rectangular study area inscribed within the stereo coverage. Albedo variations over scales resolved by the stereo starting DTM were corrected as described by Kirk et al. (2021): the orthoimage was divided by a constant-albedo simulated image computed from the DTM. This ratio image was then smoothed at the DTM resolution to remove small topographic features, yielding an albedo model. Finally, the image was divided by the albedo model. For this process to give accurate results, any overall additive contribution to image radiance (e.g., on Mars, atmospheric scattering) must first be subtracted from the observed image. We therefore fitted a linear scaling between the image and the model in which the intercept is the offset. The value was unexpectedly large. The total mean radiance factor I/F for the calibrated image was 0.0127, of which the offset comprised 0.0035 (28%) and 0.0092 was the mean surface signal.

The PC problem is formulated as the minimization of a cost function with two terms. The first is the squared difference between the observed image value and that computed from the topographic model, and the second represents a small penalty for departures from a smooth surface (i.e., for local slopes). In shadowed pixels, only the smoothness term is applied. The function is minimized iteratively by successive over- or under-relaxation applied to the linearized equations. This approach leads to local features converging more rapidly than larger ones. Each iteration adjusts elevations between neighboring pixels, so a given feature will typically converge after an iteration count that is a few times its width in pixels. To speed convergence when a low-resolution DTM is not available as a starting point, the algorithm can alternate between iterating at full and reduced resolutions. A fast initial solution based on the special properties of the equations linearized for a flat starting surface is also available (Kirk, 1987, pp. 192–196). An automated scheme to control this complex iterative process was never found, so ISIS2 program *pc2d* is interactive, allowing the user to see intermediate results and control the process. When a good starting DTM is available, it can be refined by a fixed number of relaxation steps at full resolution. This non-interactive process is implemented in the program *pcsi*.

A characteristic of PC performed with the assumption of uniform (possibly corrected) albedo is "streak" artifacts aligned with the sun (Kirk et al., 2003b). For example, an intrinsically dark patch will be (mis)interpreted as tilting away from the sun, resulting in a ridge extending from its sunward side and a trough on the down-sun side. These streaks are present in the fast initial solution and after further iteration, but they can be suppressed by tailored spatial filtering of the DTM (Kirk et al., 2003b). When iteration starts with a stereo DTM, the streaks gradually grow in length. Kirk et al. (2021) thus found that refinement of a stereo DTM typically proceeds in three phases. Over the first few

iterations, artifacts in the initial model are smoothed away, and errors decrease but resolution may degrade. In the second phase, details are added to the DTM and the resolution improves but error remains nearly unchanged. After an iteration count equal to a few times the resolution of the starting DTM, errors begin to increase as a result of the lengthening streak artifacts. Iteration should therefore be stopped at the end of the second phase.

3.4 Shape-from-shading

The ASP SfS algorithm was designed to process large numbers of images efficiently. The design allows for using overlapping images at a given point to separate topography from albedo, and for mapping broad areas in a single step with multiple images. The surface model is always defined as a DTM in ground (map) coordinates with elevation measured vertically. The cost function to be minimized has three terms: the squared difference between observed and model intensity, a term enforcing smoothness, and a term enforcing similarity to the *a priori* DTM with which iteration is started. We use smoothness and *a priori* weights of 0.04 and 0.001 except as noted. The image and smoothness terms are similar to those used in ISIS2 PC except that the image term is summed over all the images that overlap the DTM pixel. If an image pixel is determined to be shadowed (based by comparison with a user-supplied threshold), it is dropped from the cost function for that DTM cell but contributions from any other images are used, along with the smoothness and *a priori* constraints. The cost is minimized by adjusting the elevation of each DTM cell; with multiple images the albedo of each cell can also be adjusted. The ASP application *parallel_sfs* processes large DTMs by dividing them into smaller, overlapping tiles that are processed separately by the *sfs* algorithm and the results merged back together. This approach allows the use of solution algorithms that are not as efficient for large arrays as the relaxation methods used in ISIS, but that converge rapidly for features of all sizes without interactive supervision. An important point is that the shadow thresholds are used only to detect shadows and control the cost function. The offset must be subtracted from the image before using *sfs*, and if a threshold is set it is defined relative to the offset-corrected image intensities.

4. RESULTS

4.1 Stereo DTMs

As described above, all DTMs to be evaluated have a GSD of 16 m, and 16 m/pixel images were used to refine them, but initial solutions were created by stereoanalysis of 4 m/pixel images. We begin by assessing the stereo DTM at the SCH site. Figure 1a shows the RMS difference from the reference as a function of smoothing filter size. The minimum (Table 1) at about 4 DTM posts corresponds to 16 pixels in the source images. This is consistent with the result (~18 pixels) for the same matching algorithm applied to Mars images (Kirk et al., 2021). A similar scaling is expected to apply to the original images, resulting in a DTM with ~8-m resolution. Downsampled to 16 m/post this yields a reference DTM with resolution limited only by GSD.

The dispersion of the difference, however, is unexpectedly small. If it is taken to represent the expected vertical precision *EP* of the target stereopair, the value can be used to infer the RMS matching precision ρ measured in pixels, according to $EP = \rho\, GSD / (p/h)$. Based on the 4-m GSD of the downsampled images, $\rho = 0.031$ pixel, 8x smaller than the error Kirk et al. (2021) estimated when the same matcher was applied to images of Mars. Put another way, the RMS difference is close to the vertical precision we would expect for the full-resolution rather than the downsampled stereopair. A possible explanation for this discrepancy could be that because we used the same images to make both DTMs, the reference DTM contains some long-wavelength errors that are also found in the target. To assess this possibility, which would reduce the expected difference between the two DTMs, we produced an overlapping set of DTMs from the second pair listed in Section 2. Errors in these DTMs are expected to be independent from those in the first set. We made both reference and target DTMs from pair 2 and report all possible comparisons in Table 1. When we difference DTMs made from images at the same GSD (i.e., reference to reference or target to target), it is not possible to estimate resolution, but we can solve for the matching error ρ by assuming it is the same for both pairs and that the difference is the root summed square (RSS) of the two *EP* values, as appropriate for uncorrelated errors. We also allow for a factor of two reduction in the dispersion of the reference DTMs due to downsampling from their likely resolution (16 original pixels = 8 m) to 16 m/post.

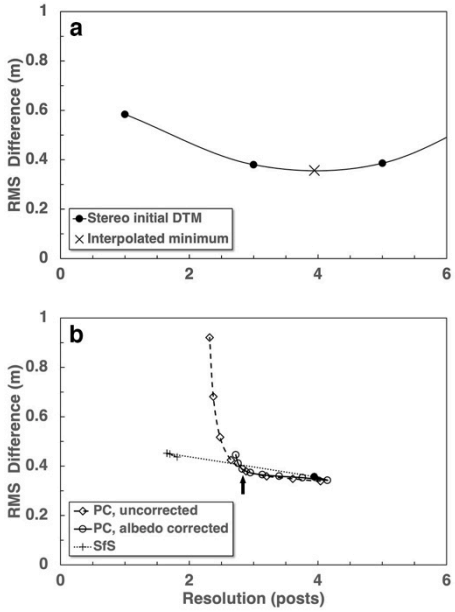

Figure 1. Quality statistics for Schrödinger site DTMs. (a) RMS difference of initial stereo DTM from reference for discrete smoothing filter sizes can be fitted by a smooth curve, with minimum indicating resolution and vertical precision. (b) Resolution and precision for DTMs refined by PC and SfS algorithms, as a function of the number of iterations. Solid dot indicates the interpolated point for initial DTM shown in (a). Arrow indicates optimal stopping point for PC iteration.

DTMs	Resolution pixels	RMS Δz m	ρ pixels
Rectangular photoclinometry area			
T_1-R_1	15.8	0.356	0.031
Overlap area between stereopairs			
T_1-R_1	16.0	0.312	0.027
T_2-R_2	16.9	0.313	0.035
T_1-R_2	15.9	0.429	0.037
T_2-R_1	17.0	0.394	0.044
T_2-T_1	—	0.387	0.027
R_2-R_1	—	0.348	0.382

Table 1. Quality statistics for stereo DTMs at the Schrödinger site. T and R refer to target and reference DTMs, respectively; subscripts refer to the stereopairs. Δz is elevation difference, ρ is matching error.

The RMS differences for the old and new pairs (reference to target) and for reference to reference and target to target compar-

isons are all similar. The slightly higher difference for pair 2 and for reference to target comparisons that mix data from the two pairs may reflect the presence of "washboard" jitter artifacts in the second stereopair, which we were only partly able to correct by spatial filtering (Kirk et al., 2003b). Thus, the matching error for the full resolution images inferred from comparing the two reference DTMs is about as expected, but the precision for the reduced images is confirmed to be unexpectedly small, disproving the idea of correlated errors. We discuss alternative explanations for this observation below. Where we can estimate resolution, the estimates from different image sets and for statistics collected over different areas are consistent to ≤6%. This lends confidence to our use of a reference DTM derived from the same images to assess the resolution improvements. Relative changes in vertical precision are expected to be reliable even though the starting value is puzzling.

4.2 Single Image with Stereo Initial DTM

Figure 1b shows the evolution of the Schrödinger DTM resolution and error (or difference with respect to the reference) as iteration proceeds with image M123668289. The behavior of *pcsi* is similar to that reported by Kirk et al. (2021) for Mars, with phases of initial smoothing, later resolution improvement, and eventual error increase. The optimal stopping point is about 32 iterations (8x the stereo DTM resolution) when the albedo-corrected image is used, but without the correction, processing should be stopped after only 8 iterations. The DTM statistics are very similar for the two cases at these stopping points, however. In particular, the resolution improvement is only a factor of 1.4, less than reported by Kirk et al. (2021). In contrast, *sfs* converges extremely rapidly and improves resolution by a factor of 2.4. Changes in quality (and in the appearance of the DTMs) are negligible after four iterations. Table 2 contains the results for both algorithms at the optimal stopping point. We emphasize that

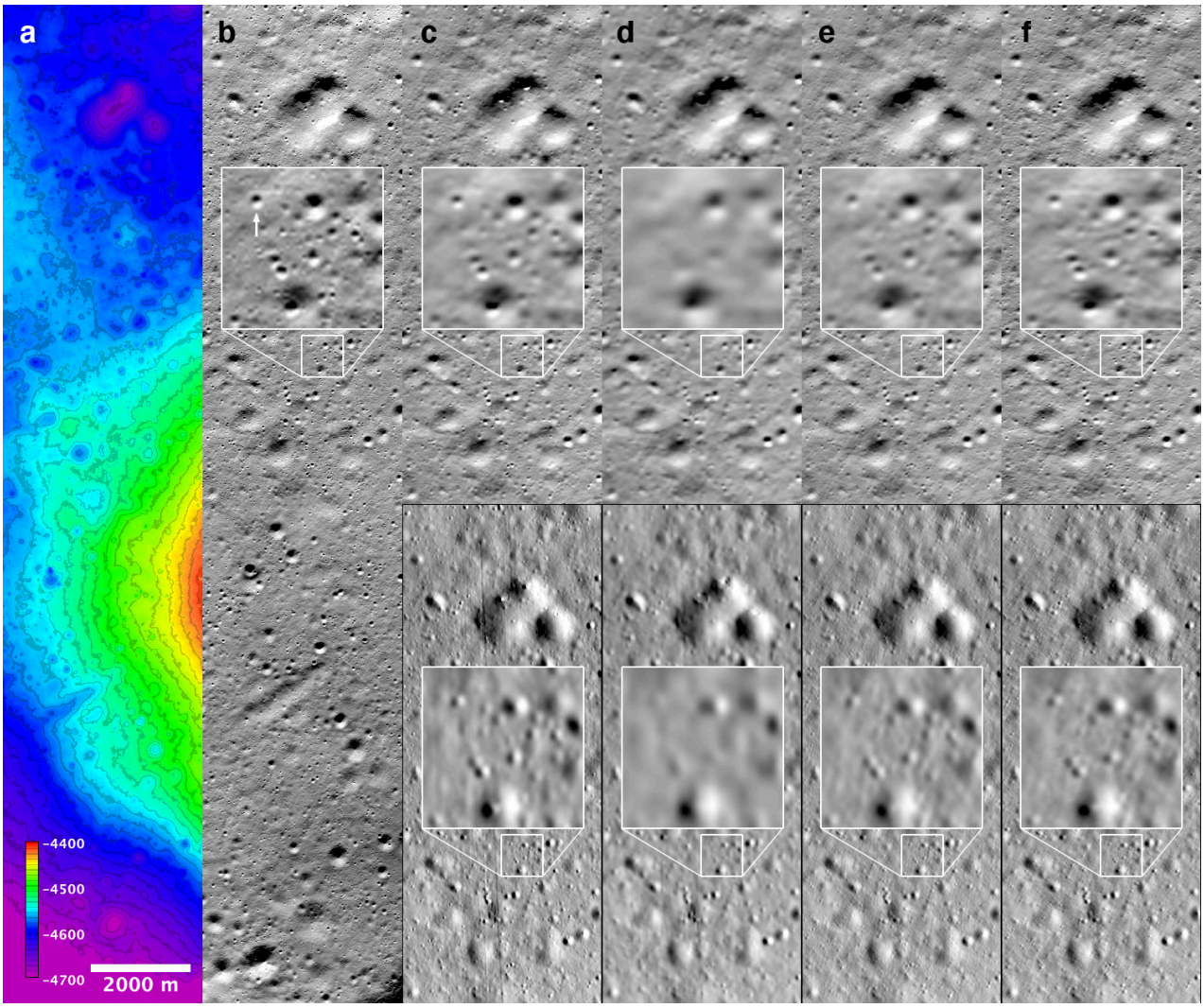

Figure 2. Comparison of DTMs at Schrödinger site. (a) Color-coded elevations from reference DTM. (b) Orthoimage M123668289. Illumination from 10° left of top. (c)-(f) Simulated images of the northern half of the DTMs, with illumination matching real image in the top row, and orthogonally from left in the bottom row to emphasize artifacts aligned with the true direction of illumination. (c) Stereo reference DTM, produced at 2 m/post from 0.5 m/pixel images and downsampled to 16 m/post. Note artifacts in shadowed areas of largest craters. (d) Initial stereo DTM, produced at 16 m/post from images downsampled to 4 m/pixel. (e) DTM after refinement by PC, 32 iterations with albedo correction based on initial DTM. (f) DTM after refinement by SfS with weights specified in text. All panels are in local Orthographic projection at 16 m/pixel with north at top. Area shown in (a) and (b) is centered near 138.3°E, 75.2°S. Boxes in (b)-(f) outline an 800x800-m area that has been enlarged to show craters at the limits of resolution. Arrow in enlarged area of image (b) indicates 80-m crater for which profiles are shown in Figure 3.

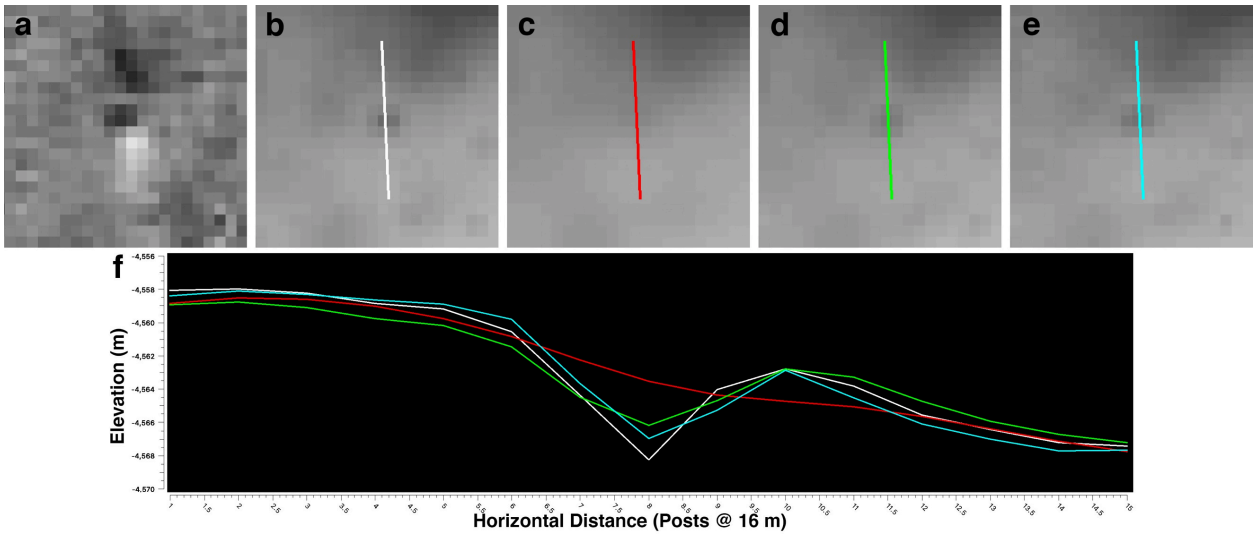

Figure 3. Appearance of a typical small (80-m diameter) crater in the DTMs. (a) Difference between SfS and PC elevations shows a maximum discrepancy of ±1 m; the alignment of this pattern with the sun direction (10° left of top) suggests slight differences in response to albedo variations or shadows. (b) Reference DTM. (c) Initial stereo DTM. (d) PC DTM. (e) SfS DTM. (f) Elevation profiles, color-coded to match colors used for profile locations in (b)-(e). Map projection same as in Figure 2. Area shown is 350 m wide.

these resolution gains were achieved with 16 m/pixel images, and that further work would be needed to show how much more improvement can be obtained by using 4-m images.

Figure 2 shows shaded relief images computed from the various DTMs. The top row of images are shaded with illumination matching the real image and can be compared; the bottom row are shaded with orthogonal illumination, which would emphasize any sun-aligned artifacts present. If such artifacts are present, they are extremely subtle. The figure confirms that the refined DTMs include small craters that appear qualitatively similar to those in the reference DTM and that are absent from the initial stereo DTM. None of the shaded images show the smallest craters present in the real image, however. This may partly be a limitation imposed by the shading process: because it is based on slopes calculated as finite differences of the DTM, it smooths the data at a scale of 2–3 posts, depending on the formula used.

An examination of the value of PC/SfS methods requires more than a qualitative demonstration of added detail. It is also essential to assess the quantitative accuracy of this detail and to characterize artifacts. To do this, we compared profiles across small features added to the DTMs by PC/SfS. The 80-m (5-post) diameter crater shown in Figure 3 is typical. This crater has a depth of 4 m in the reference DTM but is nearly absent from the initial stereo DTM. The crater appears symmetrical but slightly rounded in the refined DTMs. Its depth is underestimated by 40% by PC and 14% by SfS, likely because the crater radius is intermediate between the resolutions of the two DTMs. Depths of slightly larger craters are accurate to <10%. The PC and SfS DTMs differ by no more than ±1 m (Figure 3a); the opposite differences up- and down-sun from the crater suggest that the two algorithms are treating local albedo differences or shadows slightly differently. Excellent results were thus obtained with a single, heavily shadowed image, which is a corner case relative to the use for which *sfs* was designed. The results shown here were obtained by *not* setting a shadow threshold; setting a threshold led to flatter shadow areas, so that craters with shadows were distorted and their depths were underestimated.

A natural question is whether adjusting the weights on smoothness or the *a priori* DTM might lead to sharper or more accurate DTMs. We varied each weight separately over a wide range and found that the above results (obtained with weights of 0.04 and 0.001) could not be further improved. Increasing the smoothness weight removed detail from the DTM but decreasing it did not add detail (or introduce noise). With an *a priori* weight of 0.001, the DTM contained no visible sun-aligned artifacts (Figure 2f). Albedo cannot be modeled with a single image, but the *a priori* constraint in *sfs* limits albedo-related tilts in the DTM and forces albedo effects into the error in matching the image. The program outputs the ratio of the observed image to that simulated from the DTM as the "measured albedo." At a weight of 0.001 this ratio closely resembles the albedo map obtained as described in Section 3.3 (Figure 4a, b). The two estimates are well correlated ($r = 0.78$ after smoothing at the *a priori* DTM resolution) and the common features are geologically plausible, consisting mainly of dark crater floors, bright crater rims, and diffuse dark areas that may consist of dark pyroclastic materials (Shoemaker et al., 1994) excavated by recent craters. The "albedo" models also include banding that appears to be an instrument effect and would also distort the refined DTMs if uncorrected. Reducing the weight to 0.0001 resulted in the appearance of sun-aligned artifacts in both the DTM and albedo map (Figure 4c, d). These artifacts were more severe for weights <0.0001.

DTM	Resolution posts	RMS Δz m
Initial stereo from 4-m images	3.94	0.356
PC, albedo corrected	2.83	0.358
PC, no correction	2.88	0.379
SfS, image at 16 m/pixel	1.65	0.452
PC, no *a priori*, fast 1st approx.*	1.78	3.60
PC, no *a priori*, converged*	1.55	3.50
SfS, image at 16 m, no *a priori**†	1.11	3.80
SfS, image at 16 m, no *a priori* *‡	3.04	6.42

Table 2. Quality factors for Schrödinger site DTMs produced by PC or SFS with single image ($i = 76.9°$). All DTMs at 16-m GSD, refined with 16-m images. *A priori*/initial DTM from stereopair at 4 m/pixel unless otherwise noted. *Filtered to suppress streaks. †Processed as single tile. ‡Smoothing weight increased to 0.3.

4.3 Single Image without Stereo Initial DTM

PC/SfS methods are of interest as a potential way to obtain high resolution topography where stereo coverage is unavailable, so we tested the two algorithms without using the stereo DTM as the starting point for iteration, as a constraint, or to correct for

albedo variations. We used the offset value computed previously, however, because an accurate offset is required to obtain properly scaled results and methods to estimate it without a detailed DTM have been identified (Kirk et al., 2003a).

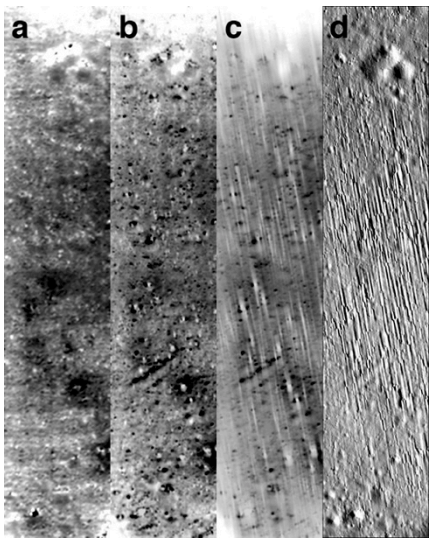

Figure 4. Albedo modelling at the Schrödinger site. (a) Albedo map for PC produced by pre-processing the image with simulated image from *a priori* DTM as described in text. (b) "Measured albedo" computed by *sfs* with *a priori* DTM weight 0.001. Contrast has been adjusted to match (a). (c) Measured albedo for *a priori* weight 0.0001. Same stretch as (b). (d) Shaded relief of DTM produced by *sfs* with *a priori* weight 0.0001. Illumination is from left; compare to Figure 3f. Reducing weight on *a priori* DTM reduces amplitude of recovered albedo variations and introduces streaks in both albedo map and DTM.

As before, we used 16-m DTMs and images. For the PC algorithm we examined the fast initial approximation and a DTM refined by iteration. As produced, the DTMs have high RMS residuals (~50 m) and are dominated by parallel streaks extending from albedo features to the edges of the DTM. We destriped the DTMs as described by Kirk et al. (2003a), highpass filtered the result with a 2-km boxcar filter, merged the result with Lunar Orbiter Laser Altimeter (LOLA; Smith et al., 2010) data that were lowpass filtered at the same scale, and evaluated quality statistics after trimming the edges of the DTM to avoid edge effects from the filters (Kirk et al., 2003b). After this processing, streaks are no longer visible in the DTM, although they can be seen in the residuals to the reference DTM. These artifacts bias the minimum RMS error towards greater smoothing of the reference DTMs, so resolution estimates PC and SfS DTMs without initial stereo were obtained by measuring artifact-free craters. As shown in Table 2, resolution and error improve slightly with iteration. Because the RMS error is dominated by larger streaks, we infer that the local precision for small features improves proportionately more.

When *sfs* is run without a detailed starting solution, the *a priori* weight must be reduced, or the larger "missing" features will not be added. As shown above, however, reducing the *a priori* weight allows sun-aligned artifacts to form. We obtained a useful result without sacrificing resolution by processing the whole DTM as a single tile, but only because this forced a compromise between areas with little albedo variation and those with more. The generic solution is to increase the smoothness weight to compensate. For the Schrödinger image, an increase from the standard 0.04 to 0.3 proved optimal, eliminating the artifacts with modest loss of resolution. As for PC, the SfS DTMs have been destriped and merged with 2-km smoothed LOLA data.

Both PC and SfS produced DTMs with resolutions comparable to or better than those obtained by refining a stereo DTM. Errors were substantially larger than with the stereo DTM as a constraint, but comparable to the ~4-m vertical precision that would be expected from a real (not downsampled) 4 m/pixel stereopair. The overall RMS error is dominated by residual sun-aligned striping, so the local precision of small features is likely to be much better than the statistic indicates. Thus, these products could be useful for many applications, and further improvement could be achieved by using the images at 4 m/pixel.

4.4 Shape-from-shading with Multiple Images

Multi-image tests were carried out at the SPA site. For brevity, we refer to image M1117557807 as N, M1158818485 as W, and M114994918 as E, indicating their approximately north, west, and east sun directions. We tested PC on N, with and without albedo correction, on a 4.48x29.44-km area within the stereo DTM. We produced DTMs by SfS from N, W, and E individually and in all combinations and evaluated them over the area where all three images overlapped. Single images were processed in *sfs* without setting a shadow threshold. Multi-image runs were performed with shadow thresholds chosen for each image and with albedo modeling enabled. Quality statistics are shown in Table 3. As in the previous sections, we used images at 16-m rather than 4-m resolution.

DTM	Resolution posts	RMS Δz m
Initial stereo from 4-m images*	4.07	0.259
PC, albedo corr. 16-m image N	2.54	0.351
PC, uncorr. 16-m image N	2.80	0.375
Initial stereo from 4-m images†	3.97	0.234
SfS, single 16-m image N	2.10	0.530
SfS, single 16-m image W	3.77	0.446
SfS, single 16-m image E	4.01	0.435
SfS, multi-image at 16 m NW	4.29	0.368
SfS, multi-image at 16 m NE	3.71	0.324
SfS, multi-image at 16 m WE	3.86	0.304
SfS, multi-image at 16 m NWE	4.15	0.325
SfS, multi-image at 16 m NWE‡	6.10	5.61

Table 3. Quality factors for SPA DTMs at 16 m/post from 4-m stereo, refined by PC/SfS with 16 m/pixel images. N, W, E indicate use of images with sun azimuths approximately north, west, and east. *Over PC study area. †Over image overlap area. ‡No *a priori*, standard weighting, filtered to suppress streaks.

The albedo-corrected PC DTM and SfS DTM from image N are of high quality, with resolutions improved by factors of 1.6 and 1.9, respectively. Crater depths are accurate to ~5%. The largest errors are associated with bright craters and ejecta, and with shadows. On the ejecta blanket of a 450-m diameter crater, which is 60% brighter than the surrounding plains, the maximum elevation errors are only 1-2 m; evidently albedo-related errors are strongly limited by the *a priori* constraint. The largest errors, approaching 10 m, are located in the shadow within this 80-m deep crater. Elsewhere, errors are mostly sub-meter.

PC without albedo correction was less successful. Albedo-related artifacts grew rapidly, limiting the number of iterations to 4 and yielding a resolution improvement of only 1.5. Single-image SfS with the higher incidence W and E images reduced the albedo-related errors compared to image N, but shadows, and thus the greater errors within them, were more extensive. We do not yet understand why using these particular images (at 16 m/pixel) did not improve the resolution of the stereo DTM.

SfS with multiple images and albedo modeling reduces the RMS error compared to the single-image cases and eliminates the

erroneous sunward tilt of bright craters and ejecta; using multiple images without modeling the albedo distribution did not improve the RMS or albedo-related errors. Multi-image SfS also yields much more accurate elevations inside craters, provided that shadow thresholds are set for each image. The maximum errors within the 450-m crater were reduced from ~10 m over most of the shadow in a single image to <5 m in small areas and less than a meter elsewhere. We discuss below why the shadow threshold is useful for multiple images but not for single images.

In the multi-image case with all three images, we were able to reduce the *a priori* weight to 0 without increasing the smoothness weight as was necessary in the single-image case. The magnitude and streaky appearance of the residuals after spatial filtering are similar to those for the *ab initio* DTM of the Schrödinger site. The horizontal resolution is not as good as for the same set of images with the *a priori* constraint, despite the smoothness weight being the same, but the degradation is only a factor of 1.5, less than the corresponding factor of 1.8 in the Schrödinger case.

5. CONCLUSIONS

This study illustrates the power of using a reference DTM to assess DTM quality. This is our first attempt to make the needed reference DTMs from the same images as the target DTMs to be evaluated, and unexpectedly good inferred precision of the initial stereo DTMs is puzzling. The results may reflect the true precision of matching between downsampled images, which have higher signal to noise ratio and less optical blur at pixel scale than images at native resolution. This hypothesis could be tested by blurring the images and/or adding noise before matching.

Our results for the improvement in DTM resolution are not expected to be affected by the starting precision, but the improvement in error for SfS may *appear* less impressive than it will be in practice. The SfS algorithm can be expected to converge to the same errors found here, even when starting with a noisier DTM. PC likely will not show as great an improvement in precision from a noisy starting solution, because it cannot eliminate the long spatial wavelength components of the error. These claims could be tested by adding noise to the starting DTM.

Quantifying the further increases in resolution obtained by using the images at the "full" resolution (as used for stereo) in PC/SfS is a logical next step to follow the present work.

Our study has highlighted the need for accurate estimates of both the shadow threshold and the image offset. Setting the threshold is useful for multi-image SfS but not for single images. This finding makes sense because a shadowed pixel provides some information about the surface but not as much as a sunlit pixel. It is therefore appropriate to ignore a shadowed pixel if there are other images, but not if the only other source of information is the *a priori* DTM. The importance of correcting the offset from atmospheric haze is well known in Mars studies, but the large offset for LROC was unexpected. Development of an efficient workflow to make these estimates would be useful, particularly for multi-image processing. In particular, the capability to estimate image offsets automatically in *sfs* could be tested. The effect of newer photometric fits of the Moon (Sato et al., 2014) on PC and SfS also warrants investigation, because changing the photometric model will change the inferred offset.

Both PC and SfS were able to improve the resolution of a stereo DTM based on a single image, although the improvement for PC was less than for SfS and less than that found by Kirk et al. (2021) for Mars images. Pre-correcting the image to reduce albedo variations was essential for PC at ~60° incidence but less important at ~80°. The *sfs* program achieved better resolution without the user effort by using the *a priori* DTM constraint to keep albedo-related errors out of the solution. For PC, the number of iterations performed is a key control parameter, and the optimum stopping point is a few times the initial DTM resolution in posts, as found by Kirk et al. (2021). For SfS, the *a priori* and smoothness weights are the main controls. Both algorithms also yielded scientifically useful DTMs from a single image without an initial stereo DTM, with error and resolution competitive with stereo (from images with 4 times smaller pixels) after the results were filtered and merged with very low-resolution data. For SfS reducing the *a priori* weight and increasing the smoothing or tile size was essential. Our results were obtained by turning off the *a priori* constraint altogether. Additional work would be beneficial to find the best weighting to make use of the valid information in a low-resolution DTM such as LOLA data while allowing *sfs* to remove artifacts and add features that the input does not resolve.

Our results show that multi-image SfS with albedo modelling can reduce vertical errors by a factor of 1.5 or more, and that with multiple images the smoothing weight does not need to be increased when the *a priori* weight is reduced. Tests with other NAC image sets could provide guidance in selecting the best combinations of images for future operational mapping. For example, SPA images at intermediate incidence angles and azimuths could be added to the current set and the optimum image criteria identified. Of even greater interest would be the investigation of multi-image SfS at other latitudes, where the available illumination conditions are qualitatively different. Near the pole, every image will be heavily shadowed, but images spanning 360° in sun azimuth could provide data for all points not in permanent shadow. The challenge may be to produce a suitable reference DTM from multiple stereopairs. At low latitudes, sun azimuths would be limited to east and west, but shadow-free images could be selected, including a low-incidence image that would strongly constrain the albedo. These ideas for image sets are not new, but making quantitative estimates of the resolution and error they yield would be an important advance.

ACKNOWLEDGEMENTS

This work was funded by the Interagency Agreement for Planetary Spatial Data Infrastructure (PSDI IAA) between the National Aeronautics and Space Administration and the U.S. Geological Survey.

REFERENCES

Alexandrov, O., Beyer, R.A., 2018. Multiview shape-from-shading for planetary images. Earth Space Sci. 5, 652-666.

Anderson, J.A., Sides, S.C., Soltesz, D.L., Sucharski, T.L., Becker, K.J., 2004. Modernization of the Integrated Software for Imagers and Spectrometers. Lunar Planet Sci. 35, 2039.

Belton, M.J.S., Klaasen, K.P., Clary, M.C., Anderson, J.L., Anger, C.D., Carr, M.H., Chapman, C.R., Davies, M.E., Greeley, R., Anderson, D., Bolef, L.K., Townsend, T.E., Greenberg, R., Head, J.W., III, Neukum, G., Pilcher, C.B., Veverka, J., Gierasch, P.J., Fanale, F.P., Ingersoll, A.P., Masursky, H., Morrison, D., Pollack, J.B., 1992. The Galileo Solid-State Imaging experiment. Space Science Reviews 60, 413-455.

Beyer, R.A., Alexandrov, O., McMichael, S., Broxton, M., Lundy, M., Husmann, K., Edwards, L., Nefian, A., Smith, B., Shean, D., Smith, T., Mstyer, Annex, A., Moratto, Z., Harguess, Aravkin, A., Meyer, J., Bhushan, S., Jlaura, 2021. NeoGeographyToolkit/StereoPipeline 3.0.0.

Bland, M., Kirk, R.L., Galuszka, D.L., Mayer, D.P., Beyer, R.A., Fergason, R.L., 2021. How well do we know Europa's

topography? An evaluation of the variability in digital terrain models of Europa. Remote Sensing 13, 4097.

Edmundson, K.L., Cook, D.A., Thomas, O.H., Archinal, B.A., Kirk, R.L., 2012. Jigsaw: The ISIS3 bundle adjustment for extraterrestrial photogrammetry. ISPRS Ann. Photogramm. Remote Sens. Spatial Inf. Sci. I-4, 203-208.

Gaddis, L., Anderson, J., Becker, K., Becker, T., Cook, D., Edwards, K., Eliason, E., Hare, T., Kieffer, H., Lee, E.M., Mathews, J., Soderblom, L., Sucharski, T., Torson, J., McEwen, A., Robinson, M., 1997. An Overview of the Integrated Software for Imaging Spectrometers (ISIS). Lunar Planet Sci. 28, 387.

Gruener, J.E., Joosten, B.K., 2009. NASA Constellation Program Office Regions of Interest on the Moon: A representative basis for scientific exploration, resource potential, and mission operations, Lunar Reconnaissance Orbiter Science Targeting Meeting, pp. 50-51.

Kirk, R.L., 1987. I Thermal evolution of a differentiated Ganymede and implications for surface features II Hydromagnetic constraints on deep zonal flows in the giant planets III A fast finite element algorithm for two-dimensional photoclinometry, Division of Geological and Planetary Sciences. California Institute of Technology, Pasadena, California.

Kirk, R.L., Barrett, J.M., Soderblom, L.A., 2003a. Photoclinometry made simple…? ISPRS Working Group IV/9 Workshop “Advances in Planetary Mapping 2003”.

Kirk, R.L., Howington-Kraus, E., Hare, T.M., Jorda, L., 2016. The effect of illumination on stereo DTM quality: Simulations in support of Europa exploration. ISPRS Ann. Photogramm. Remote Sens. Spatial Inf. Sci. III-4, 103-110.

Kirk, R.L., Howington-Kraus, E., Redding, B., Galuszka, D., Hare, T.M., Archinal, B.A., Soderblom, L.A., Barrett, J.M., 2003b. High-resolution topomapping of candidate MER landing sites with Mars Orbiter Camera narrow-angle images. J. Geophys. Res. (Planets) 108, 8088.

Kirk, R.L., Mayer, D.P., Redding, B.L., Galuszka, D.M., Fergason, R.L., Hare, T.M., Gwinner, K., 2021. Evaluating stereo digital terrain model quality at Mars Rover Landing Sites with HRSC, CTX, and HiRISE Images. Remote Sensing 13, 3511.

Laura, J.R., Beyer, R.A., 2021. Knowledge Inventory of Foundational Data Products in Planetary Science. The Planetary Science Journal 2, 18.

Malin, M.C., Bell, J.F., Cantor, B.A., Caplinger, M.A., Calvin, W.M., Clancy, R.T., Edgett, K.S., Edwards, L., Haberle, R.M., James, P.B., Lee, S.W., Ravine, M.A., Thomas, P.C., Wolff, M.J., 2007. Context Camera Investigation on board the Mars Reconnaissance Orbiter. J. Geophys. Res. (Planets) 112, E05S04.

McEwen, A.C., Becker, T., Bennett, A., Bowell, J.-A., Edwards, K., Eliason, E., Gaddis, L., Isbell, C., Howington-Kraus, A., Kirk, R.L., Lee, E., Morgan, H., Robinson, M., 1995. New Digital Images of the Moon, p. 929.

McEwen, A.S., 1991. Photometric functions for photoclinometry and other applications. Icarus 92, 298.

McEwen, A.S., Eliason, E.M., Bergstrom, J.W., Bridges, N.T., Hansen, C.J., Delamere, W.A., Grant, J.A., Gulick, V.C., Herkenhoff, K.E., Keszthelyi, L., Kirk, R.L., Mellon, M.T., Squyres, S.W., Thomas, N., Weitz, C.M., 2007. Mars Reconnaissance Orbiter's High Resolution Imaging Science Experiment (HiRISE). J. Geophys. Res. (Planets) 112, E05S02.

Miller, S.B., Walker, A.S., 1993. Further developments of Leica digital photogrammetric systems by Helava. ACSM/ASPRS Annual Convention and Exposition Technical Papers 3, 256-263.

Miller, S.B., Walker, A.S., 1995. Die Entwicklung der digitalen photogrammetrischen Systeme von Leica und Helava. Z. Photogramm. Fernerkundung 63(1), 4-16.

Neukum, G., Jaumann, R., 2004. HRSC: the High Resolution Stereo Camera of Mars Express, Mars Express: The Scientific Payload (ESA SP-1240). ESA Publications Division, ESTEC, Noordwijk, The Netherlands, pp. 17-35.

Robinson, M.S., Brylow, S.M., Tschimmel, M., Humm, D., Lawrence, S.J., Thomas, P.C., Denevi, B.W., Bowman-Cisneros, E., Zerr, J., Ravine, M.A., Caplinger, M.A., Ghaemi, F.T., Schaffner, J.A., Malin, M.C., Mahanti, P., Bartels, A., Anderson, J., Tran, T.N., Eliason, E.M., McEwen, A.S., Turtle, E., Jolliff, B.L., Hiesinger, H., 2010. Lunar Reconnaissance Orbiter Camera (LROC) instrument overview. Space Sci. Rev. 150, 81-124.

Sato, H., Robinson, M.S., Hapke, B., Denevi, B.W., Boyd, A.K., 2014. Resolved Hapke parameter maps of the Moon. Journal of Geophysical Research (Planets) 119, 1775-1805.

Shoemaker, E.M., Robinson, M.S., Eliason, E.M., 1994. The South Pole Region of the Moon as Seen by Clementine. Science 266, 1851-1854.

Sides, S.C., Becker, T.L., Becker, K.J., Edmundson, K.L., Backer, J.W., Wilson, T.J., Weller, L.A., Humphrey, I.R., Berry, K.L., Shepherd, M.R., Hahn, M.A., Rose, C.C., Rodriguez, K., Paquette, A.S., Mapel, J.A., Shinaman, J.R., Richie, J.O., 2017. The USGS Integrated Software for Imagers and Spectrometers (ISIS 3) instrument support, new capabilities, and releases. Lunar Planet Sci. 48, 2739.

Smith, D.E., Zuber, M.T., Jackson, G.B., Cavanaugh, J.F., Neumann, G.A., Riris, H., Sun, X., Zellar, R.S., Coltharp, C., Connelly, J., Katz, R.B., Kleyner, I., Liiva, P., Matuszeski, A., Mazarico, E.M., McGarry, J.F., Novo-Gradac, A.-M., Ott, M.N., Peters, C., Ramos-Izquierdo, L.A., Ramsey, L., Rowlands, D.D., Schmidt, S., Scott, V.S., Shaw, G.B., Smith, J.C., Swinski, J.-P., Torrence, M.H., Unger, G., Yu, A.W., Zagwodzki, T.W., 2010. The Lunar Orbiter Laser Altimeter Investigation on the Lunar Reconnaissance Orbiter Mission. Space Science Reviews 150, 209-241.